

Article

# A Time-History Contact Force Model of the Dynamic Load of AERORail Structures

Fangyuan Li <sup>1,\*</sup>, Zhenwei Guo <sup>1</sup>, Peifeng Wu <sup>1</sup> and Yunxuan Cui <sup>2,\*</sup>

<sup>1</sup> Department of Bridge Engineering, College of Civil Engineering, Tongji University, Shanghai 200092, China; 2132378@tongji.edu.cn (Z.G.); bridge@tongji.edu.cn (P.W.)

<sup>2</sup> School of Civil and Environmental Engineering, University of New South Wales, Sydney, NSW 2052, Australia

\* Correspondence: fyli@tongji.edu.cn (F.L.); yunxuan.cui@unsw.edu.au (Y.C.)

**Abstract:** This study proposes two curves that depict the vehicle–bridge contact force in a novel transportation system named AERORail, which is a lightweight cable-supported structure in which the rails and the prestressed cable form the load bearing system. Based on the contact force identified from a full-scale AERORail system, single and double-valley curves were obtained as the idealized contact force model for large- and small-span AERORail systems, respectively. This was achieved by utilizing the Bezier curves and the least squares method. The proposed curves were verified through a moving load model from a previous study under various spans and speeds. Moreover, the structural response of the AERORail structure under high-speed vehicle passing was explored using the idealized contact force model. The simulation results show that the proposed contact force model can predict the displacement response of 5 m and 15 m spans with a relative error of less than 5%, proving that the model can be used for dynamic analysis of AERORail.

**Keywords:** dynamic load; AERORail; flexible structure; contact force; Bezier curve; time-history load models



**Citation:** Li, F.; Guo, Z.; Wu, P.; Cui, Y. A Time-History Contact Force Model of the Dynamic Load of AERORail Structures. *Appl. Sci.* **2024**, *14*, 3055. <https://doi.org/10.3390/app14073055>

Academic Editors: Zhongxiang Liu and Tong Guo

Received: 20 February 2024

Revised: 2 April 2024

Accepted: 2 April 2024

Published: 5 April 2024



**Copyright:** © 2024 by the authors. Licensee MDPI, Basel, Switzerland. This article is an open access article distributed under the terms and conditions of the Creative Commons Attribution (CC BY) license (<https://creativecommons.org/licenses/by/4.0/>).

## 1. Introduction

The AERORail Transportation System is a new type of transportation system in the form of a cable-supported rail combined structure composed of multi-span continuous string cables, rails, lower supports and related power supply and control systems [1]. The load bearing system of AERORail consists of two rails supported by prestressed cables. AERORail is advantageous for its reduced construction cost and time, which are attributed to its simplified structure and lightweight design. A full-scale model of AERORail was reported by Li et al. [2], who studied the full-scale model's acceleration and displacement response under a two-axle vehicle. Besides the structural responses during the vibration, the contact force between the vehicle and the structure is also an intriguing topic [3,4]. Based on fundamental frequency analysis of the structure and the dynamic load test, the variation of the contact force in AERORail was studied and identified using the time domain identification method by Li et al. [5] in the previous study. It was proved that the occurrence time and frequency of the contact force are highly related to the passing time of the vehicle. However, the study was based on a limited number of experiments and was limited to low speed and 5–10 m spans. The vibration of large-span AERORail systems under high-speed vehicles is still open to discussion. Besides the absence of this knowledge, there is also a gap between the experiment data and a convincing model that depicts the variation of the contact force, which is essentially a load to the structure. Though a vehicle-structure model for the AERORail was reported by Li et al. [5], a load model applicable to static or dynamic analyses of AERORail is yet to be found. Due to the difference between the characteristics of the AERORail and conventional structures, it is necessary to investigate the contact force and devise a load model in order to promote the AERORail to its application.

The traditional way to estimate the live load to a bridge is by survey or the weigh-in-motion system [6,7]. These methods are designed to obtain the probability density of distribution for multiple vehicle types. As was discussed by Li et al. [5], the force between the vehicle and structure shows dramatic fluctuation due to the vibration, therefore the axle weight of the vehicle cannot be regarded as the contact force. The weight-in-motion system is also inapplicable for the current study due to the no-deck design of AERORail. Thus, an alternative approach must be utilized to obtain the load model based on the history of the contact force.

This paper used Bezier curves to establish a time-history load model of the AERORail structure by approximating the contact force from Li et al. [2]. The contact force was identified from the acceleration data of the structure during vehicle running. In order to validate the load model obtained, the displacement response of AERORail under the proposed load curves was compared to available experiment data. Furthermore, the structural response of large spans under high-speed vehicles was investigated via the proposed load model.

## 2. Data Fitting and Bezier Curves

Data fitting is a commonly used method in research to summarize empirical laws, which can find trend rules from measured data or simulation results simply and effectively [8,9]. For data that are discrete and random, the commonly used fitting methods include least squares, maximum likelihood estimation, etc. The least squares method refers to determining the best fit for the original data  $y(x_i)$  by choosing a function  $\hat{y}(x)$  that minimizes the sum of the squares of the differences for a given set of data [10]. This process can be represented by Equation (1):

$$e = \sum_{i=1}^N \|y(x_i) - \hat{y}(x_i)\|^2, e \rightarrow 0 \quad (1)$$

where  $e$  is the error function, and  $N$  is the total number of sample points. Generally speaking, directly obtaining the expression of the fitting function is difficult. Usually, a fitting function (Equation (2)) is determined using a set of basis functions and variable parameters:

$$\hat{y}(x) = \sum_{i=1}^N \hat{y}_i(x) \beta_i \quad (2)$$

where  $\hat{y}_i(x)$  and  $\beta_i$  are the basis functions and the variable parameters, respectively. Once the basis functions are selected, the actual problem becomes solving for  $\beta_i$ . With  $\beta_i$ , the expression of the fitting function can be obtained through Equation (2). There are various choices for the basis functions of the fitting function, including polynomial, sine function, power function, and exponential function, etc. For the contact force's time-history curve to be analyzed, due to its relatively uniform curve shape (double-valley curve or single-valley curve), traditional polynomial fitting is feasible [11,12]. However, in polynomial fitting, the physical meanings of the coefficients are not very clear, and most of the time researchers cannot derive further rules or gain any intuitive understanding of it, which hinders further in-depth research. In addition, considering that the contact force's time-history curve contains many high-frequency low-amplitude vibrations, and these have little impact on the structure because the vibrational response of the structure is mainly caused by low-frequency vibrations within its fundamental frequency range, the chosen basis function for fitting should ideally disregard this part of the vibration.

Besides polynomial and other basis functions, there are Bezier curves [13,14], B-spline curves [15,16], and non-uniform rational B-splines (NURBS) [17] available in the field of data analysis. Among these, Bezier curves have the advantages of simple form, smooth curvature, easy calculation, and easy implementation, and have been widely used in fields such as CAD, artistic design, and complex shape modeling. Bezier curves determine the

shape and position of the curve through a finite number of control points, and the visually smooth curves determined by the control points are also an important method for vector graphics. Using Bezier curves as the basis function for fitting the contact force time-history curve can effectively address the issues mentioned earlier, and Bezier curves themselves have good parameterization capabilities, making it convenient for future research to start from the curve control points and explore deeper patterns [18,19].

A Bezier curve is obtained by recursively inserting points to interpolation lines connecting consecutive control points and inserted points. For  $n + 1$  control points, one connects these points and inserts  $n$  intermediate points at a local coordinate  $t$  on each interpolation line. These intermediate points are then treated as the new control points and the above step is repeated to get new intermediate points. After the recursion, there is only one intermediate point left. If the value of  $t$  is changed (e.g., from 0.5 to 0.75), the final intermediate point will also move accordingly, thereby generating a smooth trajectory in space. This trajectory is the Bezier curve. The expression of the Bezier curve can be determined by the parameter  $t$  and the coordinates of  $n + 1$  control points (Equation (3)):

$$P(t) = \sum_{i=0}^n P_i B_{i,n}(t), \quad t \in [0, 1] \tag{3}$$

where  $P(t)$  is the expression of the Bezier curve,  $P_i$  are the coordinates of the control points,  $t$  is the independent variable parameter of the curve, and  $B_{i,n}(t)$  is the Bernstein basis function of degree  $n$  (Equation (4)):

$$B_{i,n}(t) = C_n^i t^i (1 - t)^{n-i}, \quad i = 0, 1, 2, \dots, n \tag{4}$$

If the above equation is rewritten in matrix form, it can be expressed as (Equation (5)):

$$B = \begin{pmatrix} C_n^0 C_n^0 & C_n^0 C_n^1 & \dots & C_n^0 C_n^{n-1} & C_n^0 C_n^n \\ 0 & C_n^1 C_{n-1}^0 & \dots & C_n^1 C_{n-1}^{n-2} & C_n^1 C_{n-1}^{n-1} \\ \vdots & \vdots & \vdots & \vdots & \vdots \\ 0 & 0 & \dots & C_n^{n-1} C_1^0 & C_n^{n-1} C_1^1 \\ 0 & 0 & \dots & 0 & C_n^n \end{pmatrix} \begin{pmatrix} t^0 \\ t^1 \\ \vdots \\ t^{n-1} \\ t^n \end{pmatrix} \tag{5}$$

Substituting Equation (5) into Equation (3), we obtain Equation (6):

$$P(t) = \begin{Bmatrix} x \\ y \end{Bmatrix} = PB, \quad P = \begin{Bmatrix} P_x^T \\ P_y^T \end{Bmatrix} = \begin{Bmatrix} P_{0,x} & P_{1,x} & \dots & P_{n,x} \\ P_{0,y} & P_{1,y} & \dots & P_{n,y} \end{Bmatrix} \tag{6}$$

Taking four control points as  $(0, 0)$ ,  $(10, 10)$ ,  $(20, -10)$ , and  $(30, 0)$ , the Bezier curve can be drawn as shown in Figure 1.

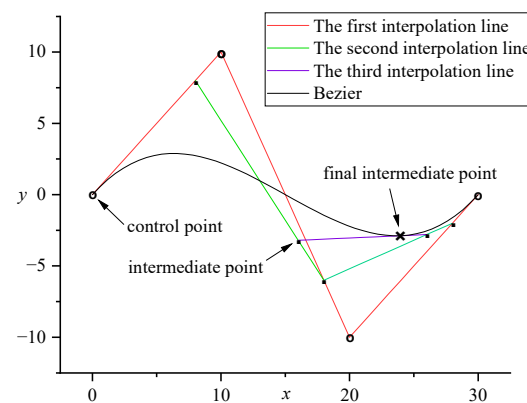


Figure 1. Bezier curve illustration.

Substituting the expression of the Bezier curve from Equation (6) into Equations (1) and (2), we can obtain the least squares fitting Equation (7) based on the Bezier curve basis function:

$$e = \sum_{i=1}^N \|y(x_i) - \mathbf{PB}\|^2, e \rightarrow 0 \quad (7)$$

Using Equation (7) to fit the contact force curve of the AERORail structure from Li et al. [2], different time-history force models can be obtained.

### 3. Time-History Contact Force Model

After analyzing the measured data from Li et al. [2], the authors obtained the time-history curves of contact forces on the elevated track under various conditions and conducted a preliminary exploration. However, if it is to be used for future elevated track design or dynamic research, the current analysis is still insufficient; more general and universally applicable results are needed. This paper establishes an ideal load model, the elevated track time-history force model, which meets the needs of elevated track design and research. It is used for calculating the deflection in different spans of an elevated track in practical applications, serving as a simplified static and dynamic calculation load for practical engineering [8,20,21]. The establishment of the time-history force model will be based on the fitting of the contact force time curves identified by the authors in Li et al. [2] from the measured data of the elevated track experimental line; for different types of contact force time curves, corresponding time-history force models will be established.

#### 3.1. Standard Double-Valley Curve Model

At a low-speed over the 5 m and 10 m spans, the time-history curves of the contact forces show two valleys, one following the other. This curve shape shows that during the vehicle's passage over the bridge, there are two impacts on the bridge, and this type of curve shape is referred to as a double-valley curve. In order to obtain a representative standard double-valley curve, this section uses the method of Bezier curve least squares described earlier to fit all double-valley curve sample data.

Although the double-valley curves are similar in shape, their duration varies with the speed of travel (as the speed decreases, the curve duration increases). The analysis results in Li et al. [2] show that there is no correlation or only a weak correlation between the statistical characteristics of the curve and speed, hence the influence of speed on the curve is only reflected in the duration. In order to eliminate the impact of speed in the standard double-valley curve, a unit duration parameter  $\tau$  is used to replace the actual time  $t$  (Equation (8)):

$$\tau = t \frac{L}{c}, \tau \in [0, 1] \quad (8)$$

Drawing the contact force curves with double-valley shapes from Li et al. [2] using the unit duration parameter, an intuitive double-valley curve sample graph is obtained (Figure 2):

The peak forces of the sample curves from Figure 2 are also given in Figure 3 for comparison.

The coordinates of the control points obtained by fitting are shown in Table 1, and the coordinate table of the control points of the standard double-valley curve.

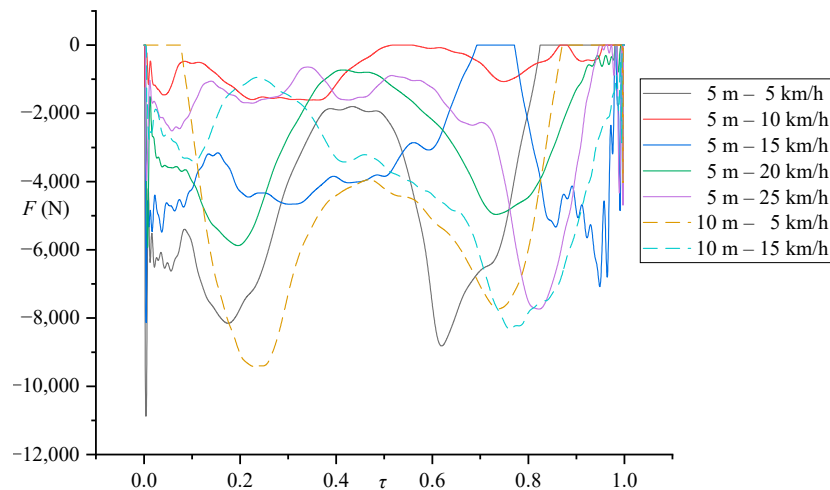


Figure 2. Sample diagram of double-valley curve.

Using Equation (7), the standard double-valley curve as shown in Figure 3 can be obtained after fitting.

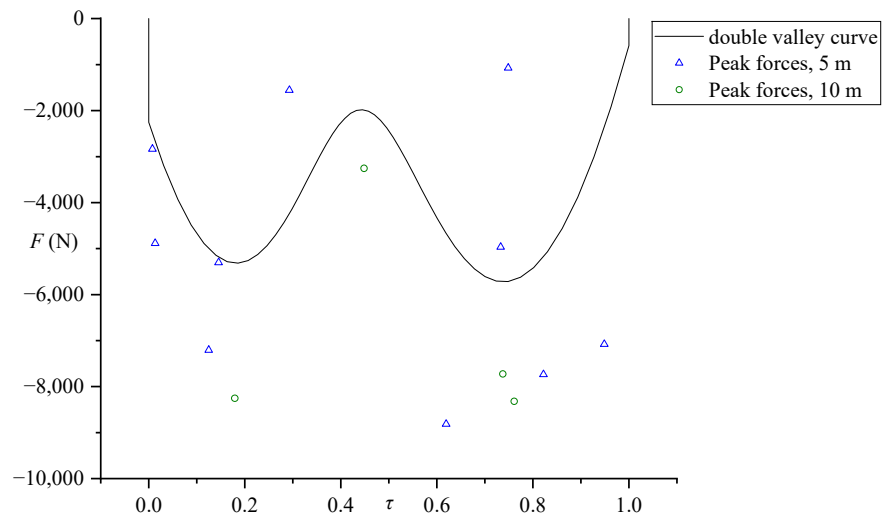


Figure 3. Standard double valley curve.

Table 1. Coordinate table of control points of standard double-valley curve.

	Units	Control Point 1	Control Point 2	Control Point 3	Control Point 4	Control Point 5
$\tau$	1	0	0.40	0.44	0.52	1
$F$	N	-2253	-15,328	17,892	-18,849	-586

### 3.2. Standard Double-Valley Curve Working Condition Recalculation

In order to verify whether the established double-valley curve can meet the needs of engineering design under the corresponding working conditions, the simplified dynamics model of AERORail established by Li et al. [5] and its Simulink simulation system were used for virtual loading. Because the double-valley curve mainly corresponds to the working condition of a 5 m span, only the corresponding working condition was simulated. The working conditions involved in the simulation are shown in Table 2.

**Table 2.** Simulation conditions of standard double-valley curve for 5 m span.

Span	m	5	5	5	5	5
Speed	km/h	5	10	15	20	25

The simulation parameters were calculated using the basic frequency of structure obtained by Li et al. [5], where the linear density of structure is given as  $\rho=55\text{ kg/m}$ . The cables of 5 m, 10 m, and 15 m spans were all prestressed by 3 tons in advance. After simulation, the mid-span deflection-time diagram under various working conditions was obtained.

The maximum mid-span deflection of each recalculation condition in Figure 4 was recorded, and the maximum deflection measured in the experiment was plotted in the figure with the operating speed as the horizontal axis, as shown in Table 3 and Figure 5.

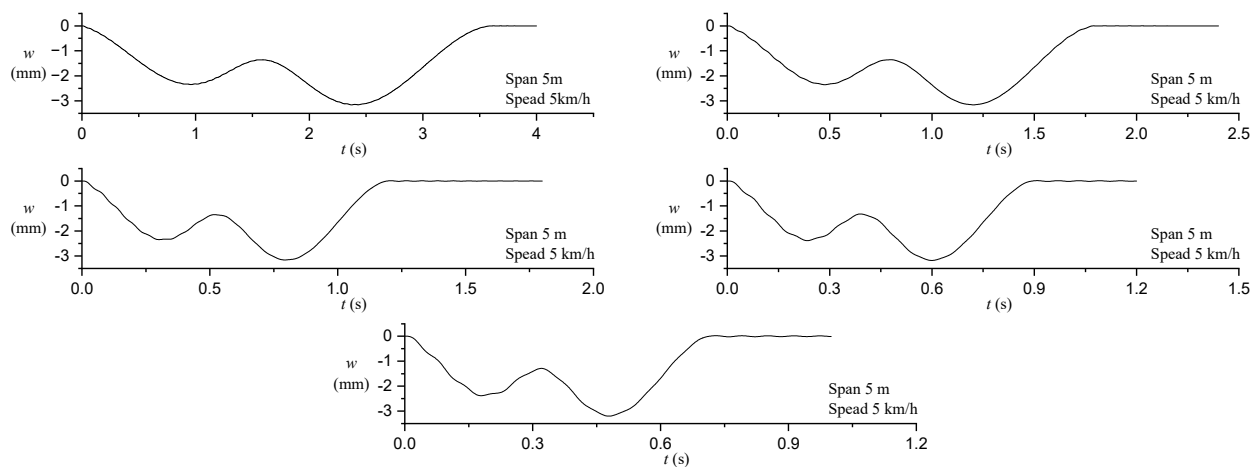


**Figure 4.** Mid-span deflection under different speed conditions of 5 m span.

**Table 3.** Maximum mid-span deflection of 5 m span.

Speed in Working Condition (km/h)	Experimental Data (mm)	Simulation Data (mm)	Relative Error (%)
5	3.27	3.16	3.36
10	3.06	3.16	3.15
15	3.28	3.16	3.66
20	3.13	3.18	1.67
25	3.47	3.20	7.76

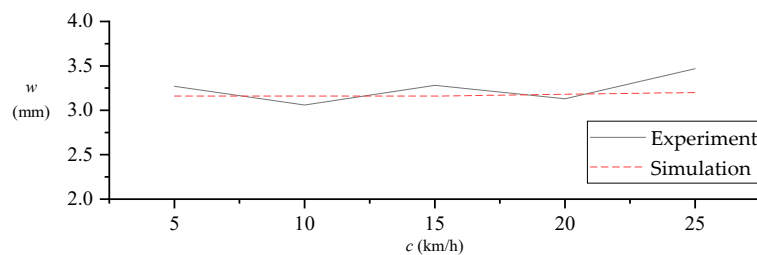


**Figure 5.** Maximum deflection in a 5 m span.

As can be seen from Table 3 and Figure 5, the numerical simulation results were relatively close to the actual experimental data at low speed, and the error was less than 4%. Under high-speed conditions, although the relative error was large, it did not increase with the increase of speed. The results show that the standard two-valley curve model has a good reference value for calculating the dynamic response of the AERORail structure

with a span of 5 m, and has a good accuracy under low speed conditions, but needs further study under high-speed conditions.

### 3.3. Standard Single-Valley Curve Model

The time-history curves of the contact forces of 10 m span under high-speed conditions have a single valley in the middle. This is also true for the contact force curves of 15 m span, regardless vehicle speed. In the same way as explained in the method in Section 3.1 above, firstly, the identified contact force time-history curves were drawn in Figure 6 with the unit duration parameter as the horizontal coordinate and the contact force as the vertical coordinate.

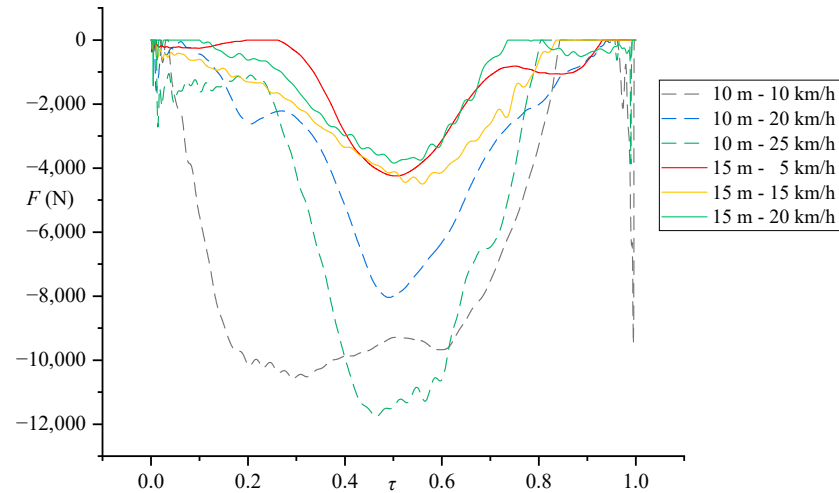


Figure 6. Sample diagram of single-valley curve.

Using Equation (7), the standard single-valley curve as shown in Figure 7 was obtained after fitting.

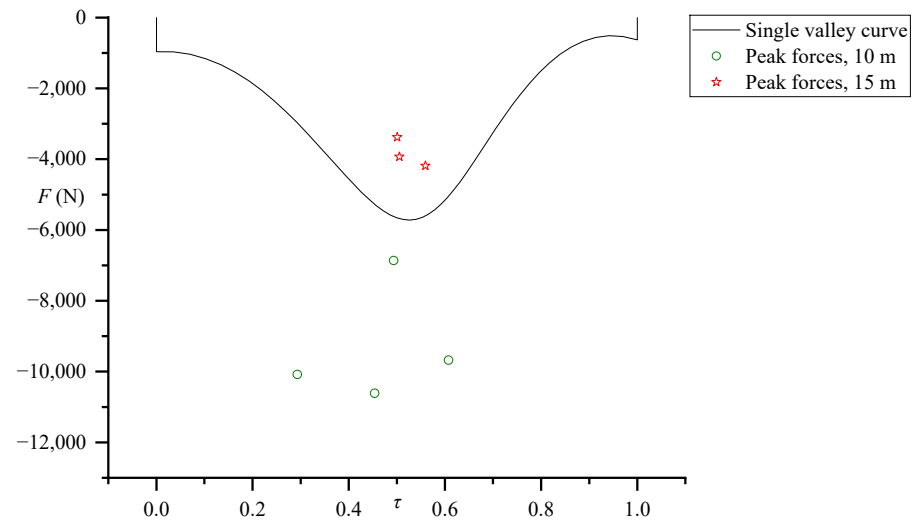


Figure 7. Standard single-valley curve.

The coordinates of the control points obtained by fitting are shown in Table 4, and the coordinates of the control points of the standard single-valley curve are shown in Table 4.

**Table 4.** Coordinate of control points of standard double-valley curve.

	Units	Control Point 1	Control Point 2	Control Point 3	Control Point 4	Control Point 5
$\tau$	1	0	0.46	0.56	0.61	1
$F$	N	-962	-587	-15,293	1129	-631

**3.4. Validation of Standard Single-Valley Curve**

In order to verify whether the established single-valley curve can meet the requirements of engineering design under the corresponding working conditions, the simplified dynamics model of AERORail established by Li et al. [5] and its Simulink simulation system were used for virtual loading. The working conditions involved in the simulation are shown in Table 5.

**Table 5.** Simulation conditions of standard double-valley curve.

Span	m	15	15	15	15
Speed	km/h	5	10	15	20

The simulation parameters were again obtained from Li et al. [5] with the obtained structure natural frequency, and take the linear density of the structure was  $\rho = 55 \text{ kg/m}$ . After simulation, the mid-span deflection time under various working conditions was obtained as shown in Figure 8.

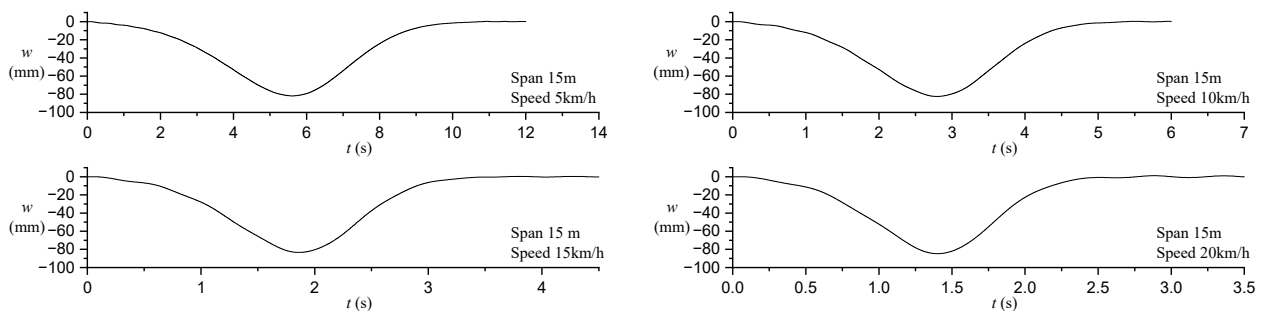


**Figure 8.** Mid-span deflection of 15 m span.

We also recorded the simulation and experimental maximum deflection value of each calculation in Figure 8, and calculated its relative error, and listed the results in Table 6 and Figure 9.

**Table 6.** Maximum deflection in 15 m span.

Speed in Working Condition (km/h)	Experimental Data (mm)	Simulation Data (mm)	Relative Error (%)
5	79.7	81.81	2.65
10	80.64	82.48	2.28
15	81.89	83.45	1.9
20	83.09	84.78	2.03

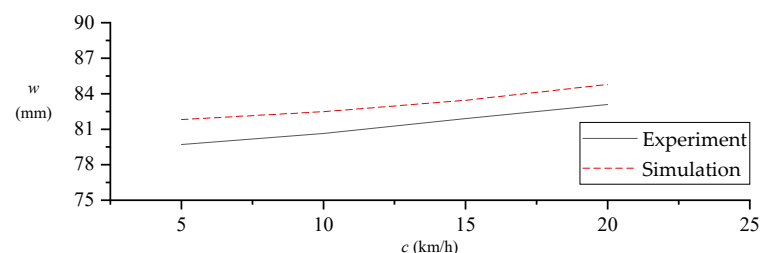


**Figure 9.** Maximum deflection in a 15 m span.

As can be seen from Table 6 and Figure 9, the numerical simulation results were relatively close to the actual experimental data at low speed, and the error was less than 3%. In all working conditions, the error remained stable, and the simulated value was stably large. This error was because the peak forces for the 15 m span were lower than the peak of the single-valley curve, as shown in Figure 7. In all cases, the single-valley curve model had a good reference value for calculating the dynamic response of the AERORail structure with a span of 15 m, and good accuracy under all working conditions.

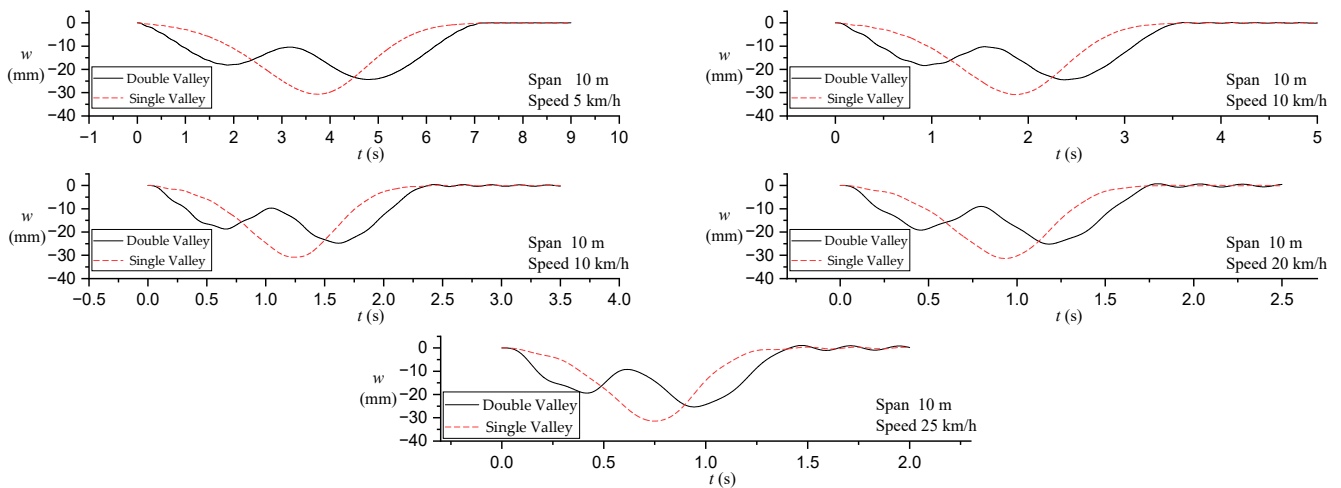
#### 4. Comparative Analysis of Models

In terms of contact force identification results, the 10 m span AERORail structure was in the alternating range of double-valley and single-valley curves. The contact force time-history curve of the low-speed working condition presented a double-valley curve form, while the high-speed working condition presented a single-valley curve form. In order to clarify the most accurate ideal force model under different speed conditions over a 10 m span, and further study the difference between the calculation results of the standard double-valley curve and the standard single-valley curve over the same span and the same speed, this section used the simulation system to double-calculate the five speed conditions over a 10 m span by using two curve models respectively. The working conditions involved in the simulation are shown in Table 7.

**Table 7.** Simulation conditions of standard single-valley curve.

Span	m	10	10	10	10	10
Speed	km/h	5	10	15	20	25

The simulation parameters were still the same as in Li et al. [5]. The basic frequency of the structure was calculated and the quality of the structure line was taken as  $\rho = 55 \text{ kg/m}$ . After simulation, the mid-span deflection time under various working conditions was obtained as shown in Figure 10.

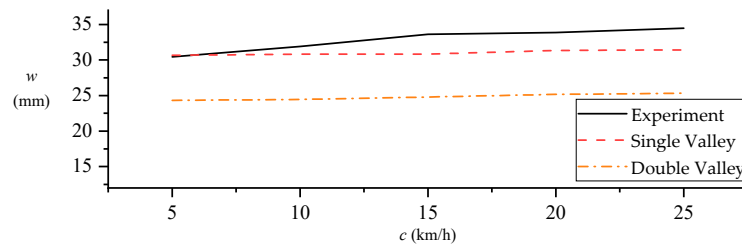


**Figure 10.** Recalculation of 10 m span working conditions.

The maximum mid-span deflection obtained in Figure 10 was compared with the maximum mid-span deflection measured in the experiment, and the results shown in Table 8 and Figure 11 were obtained.

**Table 8.** Maximum mid-span deflection of 10 m span.

Speed in Working Condition (km/h)	Experimental Data (mm)	Single-Valley Simulation (mm)	Relative Error (%)	Double-Valley Simulation (mm)	Relative Error (%)
5	30.45	30.67	0.73	24.32	20.12
10	31.92	30.82	3.42	24.45	23.39
15	33.61	30.84	8.24	24.79	26.25
20	33.86	31.35	7.42	25.17	25.65
25	34.49	31.42	8.88	25.32	26.57

**Figure 11.** Maximum deflection over a 10 m span.

As can be seen from Table 8 and Figure 11, the numerical simulation results of the standard single-valley curve were relatively close to the actual experimental data, with an error of less than 9%. The error was small at low speed, but increased with the increase of speed, and finally fluctuated around 8%. Again, this error was caused by the different peaks in the single-valley curve model and the samples, as illustrated in Figure 7. The peaks for 10 m spans were higher than in the single-valley curve model, which led to the underestimation of deflection in the simulation.

The standard double-valley curve deviated greatly from the experimental value under all working conditions, and the simulated value was stably small, which indicates that the standard double-valley curve is not suitable for the calculation of a 10 m span, unless some correction is made. In general, the single-valley curve model has a certain reference value for calculating the dynamic response of the AERORail structure with a span of 10 m, and has relatively stable accuracy under all working conditions.

## 5. Calculation of High-Speed Working Conditions

In the design concept of the AERORail, the final design of the AERORail transportation system can reach 100~300 km/h. However, due to the limited conditions, the existing scale model experiment and experimental line experiment could not completely simulate such a high speed. Therefore, it was important to use the existing numerical simulation system and ideal load model to predict the possible high-speed working conditions and analyze the possible resonance of the bridge qualitatively. In this section, the standard single-valley curve model and standard double-valley curve model in Section 2 were used to simulate 5 m, 10 m and 15 m span AERORail structures in the speed range of 40~300 km/h. The simulation calculation of a 30 m long AERORail structure without measured data was carried out.

### 5.1. Short Span High-Speed Working Condition Simulation

The calculation parameters of 5 m, 10 m, and 15 m span AERORail structures were as described by Li et al. [5] and Section 2. The working conditions involved in the simulation are shown in Table 9:

**Table 9.** High-speed simulation working conditions table.

Speed km/h \ Span m	40	60	80	100	120	150	200	250	300
5	Double valley								
10	Single valley								
15	Single valley								

Considering that the standard double-valley curve model had satisfactory accuracy in the simulation of a 5 m span, the standard double-valley curve model was used to calculate the 5 m span AERORail structure. The calculated mid-span deflection-time curve is shown in Figure 12.

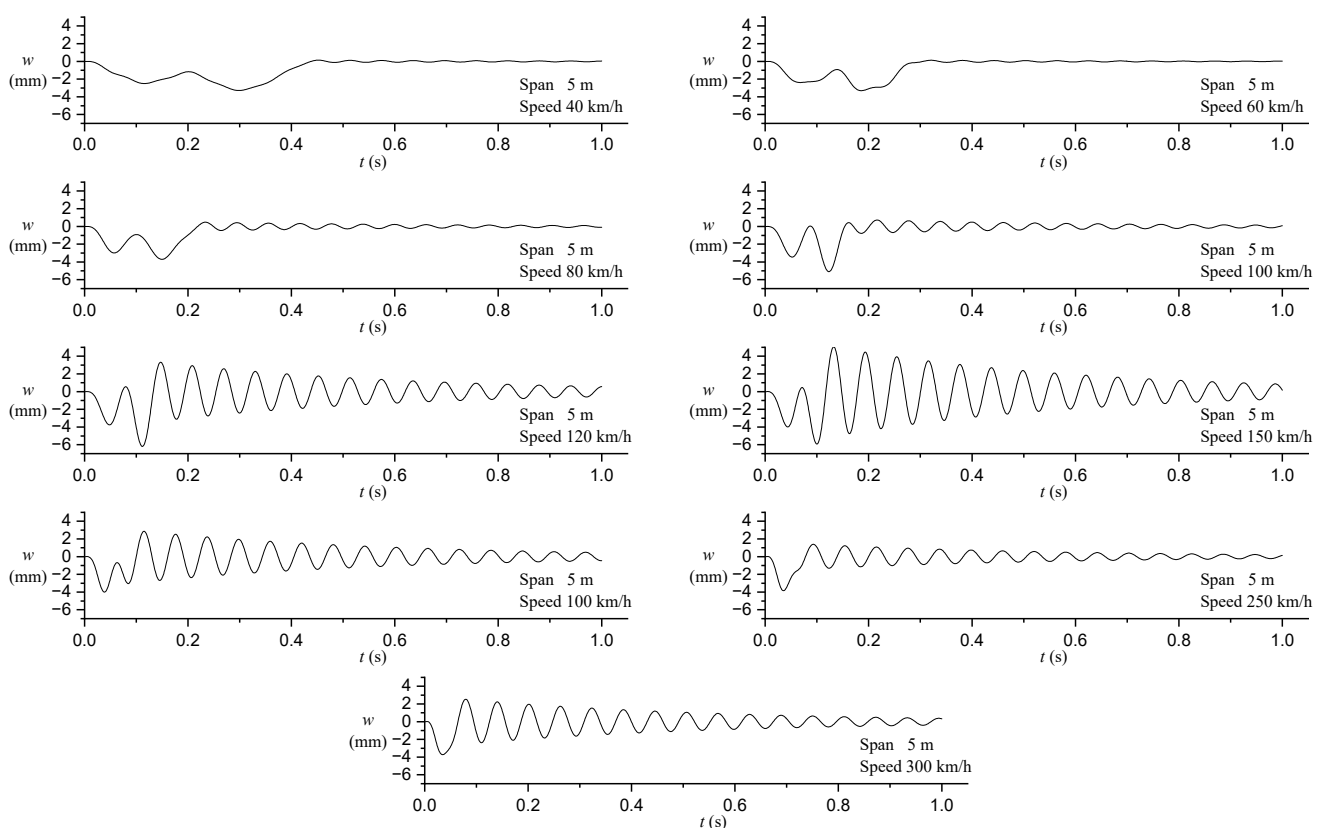


**Figure 12.** Simulation of high-speed working condition of 5 m span.

The simulation results in Figure 12 showed the following. (1) With the increase of speed, the residual vibration amplitude retained by the AERORail structure after excitation increased continuously. (2) When the speed was greater than 100 km/h, the rebound in the AERORail span became more and more obvious. (3) With the increase of speed, the two extremes of deflection generated by the two-valley curve gradually approached each other and finally merged into a single extreme value (300 km/h, 3.73 mm). (4) The condition with the maximum deflection was not the condition with the highest speed, and the extreme deflection increased first and then became smaller with the increase of speed, reaching a maximum value of 6.19 mm around 120 km/h. (5) When the speed was greater than 250 km/h, the vibration response of the AERORail was close to damped free vibration.

According to the above results, the following conclusions can be drawn: (1) the dynamic response of a 5 m span under high-speed conditions gradually approached the

response of a damped free vibration system with the increase of speed; (2) the resonance speed of a 5 m span was near 120 km/h; (3) the maximum dynamic deflection of a 5 m span under the action of a standard double-valley curve model was about 6.19 mm.

For the simulation of 10 m and 15 m spans, considering that the standard single-valley curve model had high calculation accuracy under these two span structures, and the contact force history curve itself was close to the single-valley curve shape under high-speed working conditions, the time force model used in the calculation of 10 m and 15 m spans was the standard single-valley curve model. The calculation results of the 10 m span under high-speed working conditions can be seen in Figure 13.

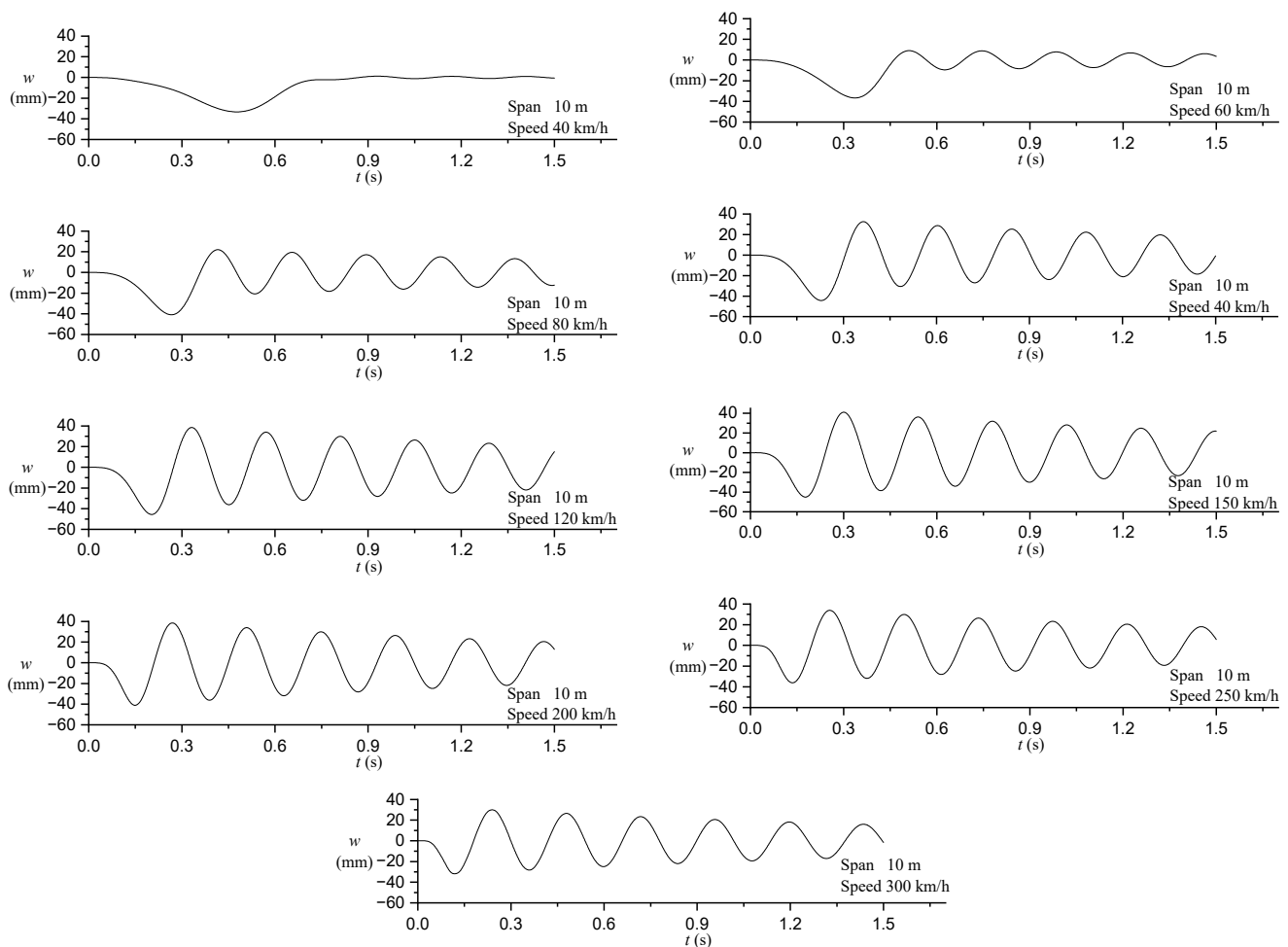


**Figure 13.** Simulation of high-speed working conditions of a 10 m span.

The simulation results of the 10 m span high-speed working conditions had the following characteristics. (1) With the increase of speed, the residual vibration amplitude retained by the AERORail structure after excitation increased continuously. (2) When the speed was greater than 40 km/h, the rebound in the AERORail span became more and more obvious. (3) The condition of maximum deflection was similar to that of the 5 m span, but not the condition of highest speed. The extreme value of deflection increased first and then became smaller with the increase of speed, reaching a maximum value of 45.63 mm around 120 km/h. (4) When the speed was greater than 80 km/h, the vibration response of the AERORail was close to damped free vibration.

According to the above characteristics, the following conclusions can be drawn. (1) The dynamic response of the 10 m span under high-speed conditions gradually approached the response of a damped free vibration system with the increase of speed. (2) The resonant speed of the 10 m span was between 100 km/h and 150 km/h. (3) The maximum dynamic

deflection of the 10 m span under the action of a standard single-valley curve model was not less than 45.63 mm.

The calculation results of high-speed working conditions of the 15 m span can be seen in Figure 14.

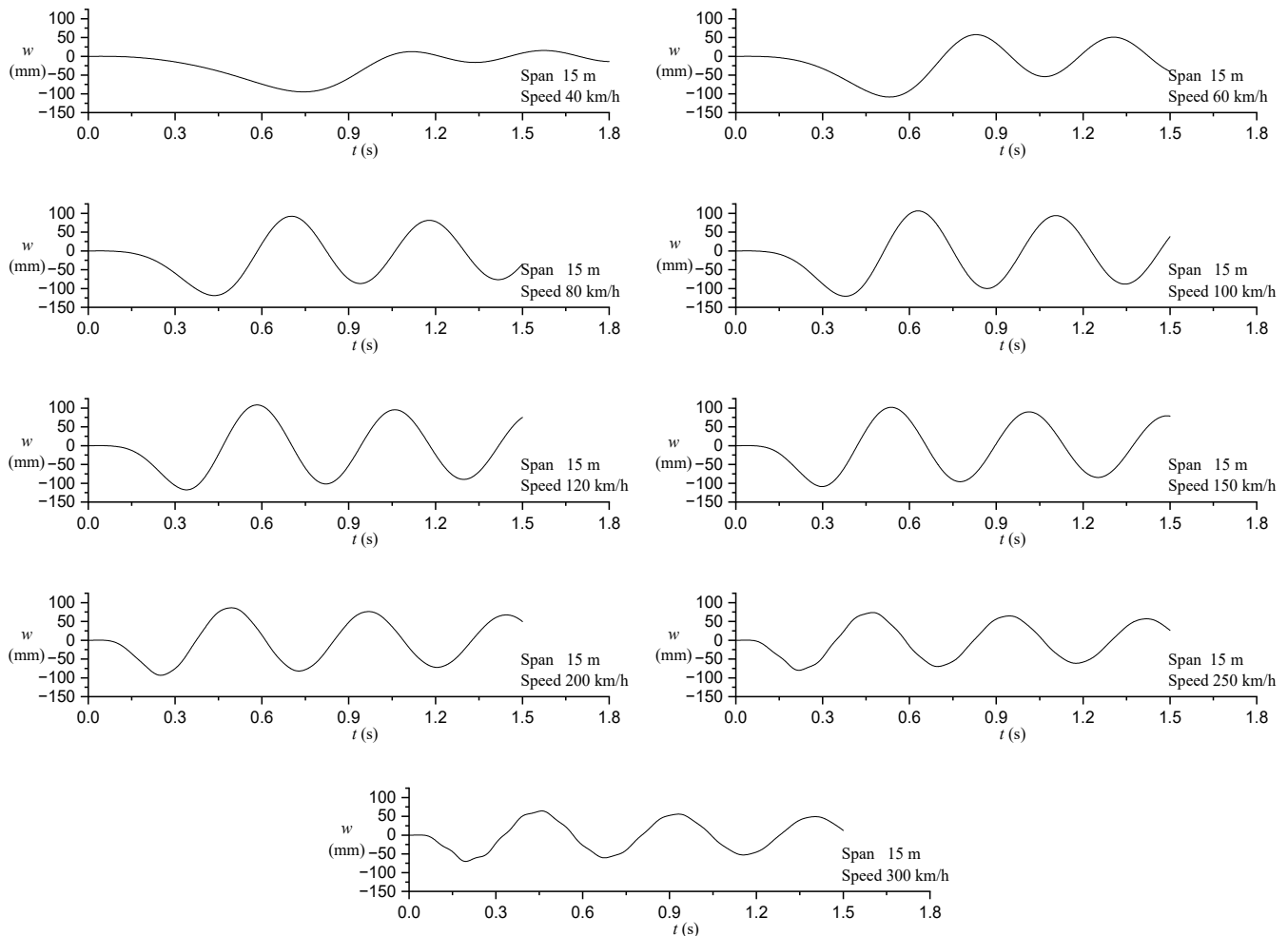


**Figure 14.** Simulation of high-speed working conditions of the 15 m span.

The simulation results of the 15 m span under high-speed conditions had the following characteristics. (1) With the increase of speed, the residual vibration amplitude retained by the AERORail structure after excitation increased first, and then decreased. (2) When the speed was greater than 40 km/h, the rebound in the AERORail span became more and more obvious. (3) The condition of maximum deflection was similar to that of the 5 m span, but not the condition of highest speed. The extreme value of deflection increased first and then became smaller with the increase of speed, reaching a maximum value of 120.48 mm at about 100 km/h. (4) When the speed was greater than 60 km/h, the vibration response of the AERORail was close to that of damped free vibration. (5) When the speed was greater than 250 km/h, the deflection curve started to exhibit local fluctuation.

### 5.2. Simulation of High Speed of 30 m Span

In order to study the dynamic characteristics of the AERORail structure with a larger span, this section carried out the simulation of a 30 m span AERORail structure to obtain its dynamic response under a moving point load. The magnitude of the point load was determined by the single-valley curve. This 30 m span of AERORail was similar to the 15 m span in structure. Three support rods were set on each side connecting the rail and the prestressed cable. The lengths of the three support rods were 40 cm, 54 cm, and 40 cm,

respectively. The tensile force of the cable was the same as the tensile force (3 tons) used in the test line. Before simulation, the 30 m span structure was also established using the finite element model and its natural frequency was calculated (Table 10).

**Table 10.** Natural frequency of vertical vibration of 30 m span.

Span	Cable Tension	Natural Frequency of Vertical Vibration in Hz					
		$f_1$	$f_2$	$f_3$	$f_4$	$f_5$	$f_6$
30 m	3 tons	1.13	2.05	4.16	7.37	10.93	15.56

The standard single-valley curve model load was used to test the 30 m span AERORail. The speed conditions involved in the calculation and the maximum span deflection within the working conditions are shown in Table 11.

**Table 11.** Working conditions and calculation results for 30 m span.

Speed (km/h)	1	5	10	15	20	25	40	60	80	100	120	150	200	250	300
Deflection (mm)	147.1	147.3	147.9	149.0	150.7	154.7	166.8	185.3	200.8	202.7	196.0	183.3	164.4	144.4	125.4

The mid-span deflection-time history curve of the 30 m span AERORail can be seen as shown in Figure 15.

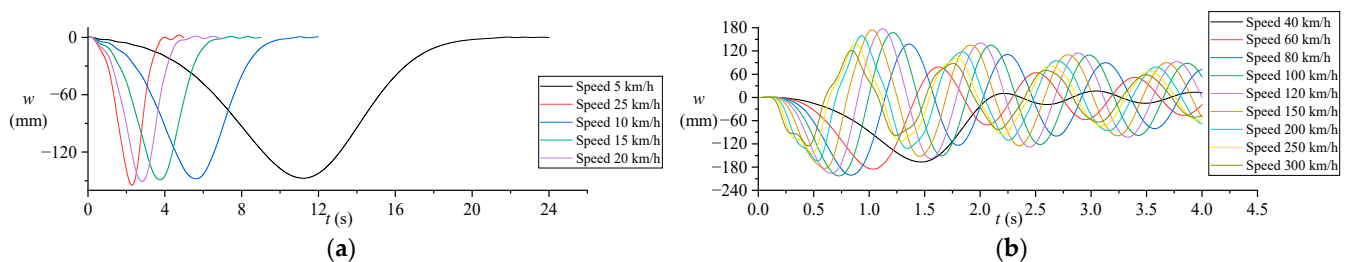


**Figure 15.** Simulation of mid-span deflection under different speed conditions of 30 m span. (a) Speed less than 25 km/h; (b) speed greater than 40 km/h.

The simulation results of the 30 m span working conditions had the following characteristics. (1) With the increase of speed, the residual vibration amplitude retained by the AERORail structure after being excited first increased and then decreased. (2) When the speed was less than 25 km/h, the impact effect of dynamic load was not obvious, and the deflection of the AERORail was close to that of a static load. (3) When the speed was greater than 25 km/h, the dynamic response of the AERORail became obvious, and when the speed was greater than 40 km/h, the rebound in the span of the AERORail became more and more obvious. (4) The condition with the maximum deflection was similar to the conditions for 5 m, 10 m, and 15 m spans, but was not the condition with the highest speed. The extreme value of deflection increased first and then became smaller with the increase of speed, reaching a maximum value of 202.7 mm around 100 km/h. (5) When the speed was greater than 100 km/h, the vibration response of the AERORail was close to damped free vibration. (6) When the speed was greater than 150 km/h, the deflection curve began to show certain local fluctuation.

## 6. Conclusions

The present study explored a way to devise live load models for a novel transportation system called AERORail based on the vehicle–structure contact force identified from structure’s acceleration data. The identified contact forces were grouped and then fitted

using Bezier curves and the least-squares method. The resultant two force models, namely the single-valley and double-valley curves, were validated in a Simulink model against the experiment data under five different vehicle speeds and three span lengths. The simulations showed that the proposed load model gave a good prediction of the mid-span deflection; therefore the established standard load models can be used for the dynamic analysis of AERORail. The conclusions are as follows.

(1) The live load for the lightweight AERORail can be obtained by fitting the identified contact force using Bezier curves. The resultant load curve can be used to predict the dynamic displacement response of the structure.

(2) The variation in span length leads to the different shape of the load curve. The load models for 5 m and 15 m span AERORails have one- and two-peak magnitudes, respectively. The variation of speed mainly affects the magnitude rather than the shape of the load curve.

Aside from the existing research on small-span AERORails and low-speed vehicles, this article also discusses the dynamic deflection of a 30 m AERORail with vehicle speed of 40–300 km/h. It was found from the simulation that:

(3) The resonant speed of the 30 m span was between 80 km/h and 100 km/h, which was less than that of the 5 m, 10 m, and 15 m spans. At speeds of about 150 km/h and above, higher-order vibration components began to appear. This phenomenon should be carefully considered in future design and research of AERORail.

The current study designed load models for AERORail. However, the methodology applied in the article can also benefit the load model study on other prestressed bridge structures.

**Author Contributions:** Conceptualization, F.L. and P.W.; methodology, Z.G., Y.C. and P.W.; validation, Z.G. and Y.C.; formal analysis, Z.G. and Y.C.; writing—original draft preparation, Z.G. and Y.C.; writing—review and editing, F.L.; visualization, Z.G.; supervision, F.L.; project administration, F.L.; funding acquisition, F.L. All authors have read and agreed to the published version of the manuscript.

**Funding:** This research was supported by the National Natural Science Foundation of China (Grant No. 50708072, No. 51378385) and was supported by the Fundamental Research Funds for the Central Universities of China (Grant No. 22120180318).

**Institutional Review Board Statement:** Not applicable.

**Informed Consent Statement:** Not applicable.

**Data Availability Statement:** The original contributions presented in the study are included in the article, further inquiries can be directed to the corresponding authors.

**Conflicts of Interest:** The authors declare that they have no conflict of interest.

## References

- Li, F.; Liu, D.J.; Han, J.B.; Wang, J.L. Structure form of pretension string rail structure and application prospect. In *Structures and Architecture*; Cruz, P.J.S., Ed.; CRC Press: Boca Raton, FL, USA, 2010; pp. 1546–1553.
- Li, F.; Guo, Z.; Cui, Y.; Wu, P. Dynamic Load Test and Contact Force Analysis of the AERORail Structure. *Appl. Sci.* **2023**, *13*, 2011. [[CrossRef](#)]
- Aloisio, A.; Alaggio, R. Probabilistic Comparative Analysis of Vehicle–Bridge Interaction Models for Predicting Bridge Response under Moving Vehicles. *J. Eng. Mech.* **2024**, *150*, 04023121. [[CrossRef](#)]
- Shi, Z.; Mohammed, Y.M.; Uddin, N.; Chen, G. A vehicle-bridge interaction model considering contact patch size and vehicle self-generated excitation—A theoretical study. *Eng. Struct.* **2024**, *298*, 117079. [[CrossRef](#)]
- Li, F.-Y.; Guo, Z.-W.; Cui, Y.-X.; Wei, S.-H. Dynamic Numerical Simulation Model and Time-Domain Identification of Flexible AERORail Structure. *Shock. Vib.* **2023**, *2023*, 2227785. [[CrossRef](#)]
- Nowak, A.S. Live load model for highway bridges. *Struct. Saf.* **1993**, *13*, 53–66. [[CrossRef](#)]
- Chen, B.; Zhong, Z.; Xie, X.; Lu, P. Measurement-Based Vehicle Load Model for Urban Expressway Bridges. *Math. Probl. Eng.* **2014**, *2014*, 340896. [[CrossRef](#)]
- Liu, R.; Dobriban, E.; Hou, Z.; Qian, K. Dynamic Load Identification for Mechanical Systems: A Review. *Arch. Comput. Methods Eng.* **2021**, *29*, 831–863. [[CrossRef](#)]
- Li, Z.Y.; Zhu, C.F. Dynamic load identification method based on functional principle. *Foreign Electron. Meas. Technol.* **2020**, *39*, 51–54. [[CrossRef](#)]

10. Jiang, J.; Luo, S.; Zhang, F. One novel dynamical calibration method to identify two-dimensional distributed load. *J. Sound Vib.* **2021**, *515*, 116465.
11. Gao, W.; Ren, Z. Dynamic load identification based on piecewise fitting trend term and smooth curve. *J. Phys. Conf. Ser.* **2022**, *2364*, 012049.
12. Yang, H.J.; Jiang, J.H.; Chen, G.P.; Zhao, J.M. Dynamic load identification based on deep convolution neural network. *Mech. Syst. Signal Process.* **2023**, *185*, 109757. [[CrossRef](#)]
13. Mineur, Y.; Lichah, T.; Castelain, J.M.; Giaume, H. A shape controlled fitting method for Bézier curves. *Comput. Aided Geom. Des.* **1998**, *15*, 8789–8891. [[CrossRef](#)]
14. Zhou, L.S.H. Curve Fitting with Bézier Cubics. *Graph. Models Image Process.* **1996**, *58*, 223–232.
15. Park, H.; Lee, J.H. B-spline curve fitting based on adaptive curve refinement using dominant points. *Comput. Aided Des.* **2007**, *39*, 439–451. [[CrossRef](#)]
16. Zheng, W.; Bo, P.; Liu, Y.; Wang, W. Fast B-spline curve fitting by L-BFGS. *Comput. Aided Geom. Des.* **2012**, *29*, 448–462. [[CrossRef](#)]
17. Tiller, L.P.W. *The NURBS Book*; Springer Science & Business Media: Berlin, Germany, 2012.
18. Yan, Z.; Teng, S.; Luo, W.; Bassir, D.; Chen, G. Bridge Modal Parameter Identification from UAV Measurement Based on Empirical Mode Decomposition and Fourier Transform. *Appl. Sci.* **2022**, *12*, 8689. [[CrossRef](#)]
19. Lorenzoni, F.; Conto, N.D.; Porto, F.d.; Modena, C. Ambient and free-vibration tests to improve the quantification and estimation of modal parameters in existing bridges. *J. Civ. Struct. Health Monit.* **2019**, *9*, 617–637. [[CrossRef](#)]
20. Feng, F.; Huang, F.; Wen, W.; Liu, Z.; Liu, X. Evaluating the Dynamic Response of the Bridge-Vehicle System considering Random Road Roughness Based on the Moment Method. *Adv. Civ. Eng.* **2021**, *2021*, 9923592.
21. Michael, V.; Rune, B.; Christos, G. Evaluating the Effect of Modelling Errors in Load Identification Using Classical Identification Methods. *Shock. Vib.* **2019**, *2019*, 9490760.

**Disclaimer/Publisher’s Note:** The statements, opinions and data contained in all publications are solely those of the individual author(s) and contributor(s) and not of MDPI and/or the editor(s). MDPI and/or the editor(s) disclaim responsibility for any injury to people or property resulting from any ideas, methods, instructions or products referred to in the content.